



Providing Choice & Value

Generic CT and MRI Contrast Agents



CONTACT REP

AJNR

This information is current as of July 19, 2025.

Predicting Antiseizure Medication Treatment in Children with Rare Tuberous Sclerosis Complex–Related Epilepsy Using Deep Learning

Haifeng Wang, Zhanqi Hu, Dian Jiang, Rongbo Lin, Cailei Zhao, Xia Zhao, Yihang Zhou, Yanjie Zhu, Hongwu Zeng, Dong Liang, Jianxiang Liao and Zhicheng Li

AJNR Am J Neuroradiol 2023, 44 (12) 1373-1383

doi: <https://doi.org/10.3174/ajnr.A8053>

<http://www.ajnr.org/content/44/12/1373>

Predicting Antiseizure Medication Treatment in Children with Rare Tuberous Sclerosis Complex–Related Epilepsy Using Deep Learning

 Haifeng Wang,  Zhanqi Hu,  Dian Jiang,  Rongbo Lin,  Cailei Zhao,  Xia Zhao, Yihang Zhou,  Yanjie Zhu,  Hongwu Zeng,  Dong Liang,  Jianxiang Liao, and  Zhicheng Li

ABSTRACT

BACKGROUND AND PURPOSE: Tuberous sclerosis complex disease is a rare, multisystem genetic disease, but appropriate drug treatment allows many pediatric patients to have positive outcomes. The purpose of this study was to predict the effectiveness of antiseizure medication treatment in children with tuberous sclerosis complex–related epilepsy.

MATERIALS AND METHODS: We conducted a retrospective study involving 300 children with tuberous sclerosis complex–related epilepsy. The study included the analysis of clinical data and T2WI and FLAIR images. The clinical data consisted of sex, age of onset, age at imaging, infantile spasms, and antiseizure medication numbers. To forecast antiseizure medication treatment, we developed a multitechnique deep learning method called WAE-Net. This method used multicontrast MR imaging and clinical data. The T2WI and FLAIR images were combined as FLAIR3 to enhance the contrast between tuberous sclerosis complex lesions and normal brain tissues. We trained a clinical data-based model using a fully connected network with the above-mentioned variables. After that, a weighted-average ensemble network built from the ResNet3D architecture was created as the final model.

RESULTS: The experiments had shown that age of onset, age at imaging, infantile spasms, and antiseizure medication numbers were significantly different between the 2 drug-treatment outcomes ($P < .05$). The hybrid technique of FLAIR3 could accurately localize tuberous sclerosis complex lesions, and the proposed method achieved the best performance (area under the curve = 0.908 and accuracy of 0.847) in the testing cohort among the compared methods.

CONCLUSIONS: The proposed method could predict antiseizure medication treatment of children with rare tuberous sclerosis complex–related epilepsy and could be a strong baseline for future studies.

ABBREVIATIONS: ACC = accuracy; ASM = antiseizure medication; AUC = area under the curve; CNN = convolutional neural network; DCA = decision curve analysis; FCNN = fully connected neural network; FN = false-negative; FP = false-positive; ReLU = rectified linear unit; ROC = receiver operating characteristic; SEN = sensitivity; SPE = specificity; TN = true-negative; TP = true-positive; TSC = tuberous sclerosis complex; WAE = weighted-average ensemble

Tuberous sclerosis complex (TSC) is a rare genetic disease that affects multiple organs and is caused by mutations in the *TSC1* or *TSC2* genes.^{1–3} Its incidence is estimated to be 1 in 6000 live births,^{3,4} and it is commonly associated with seizures and related neuropsychiatric disorders.⁵ Epilepsy is the most prevalent symptom in pediatric patients with TSC,^{6,7}

affecting approximately 85% of them.^{2,8} The primary objective of epilepsy treatment in these patients is to control seizures and enhance their quality of life.³ However, >50% of pediatric patients with TSC develop drug resistance to antiseizure medication (ASM),^{9–11} and identifying this resistance can be a time-consuming process.¹² Therefore, investigating predictive

Received June 4, 2023; accepted after revision October 3.

From the Research Center for Medical Artificial Intelligence (H.W., D.J., Y. Zhou, D.L., Z.L.) and Paul C. Lauterbur Research Center for Biomedical Imaging (Y. Zhu, D.L.), Shenzhen Institutes of Advanced Technology, Chinese Academy of Sciences, Shenzhen, Guangdong, China; Shenzhen College of Advanced Technology (H.W., D.J., Y. Zhu, D.L., Z.L.), University of Chinese Academy of Sciences, Shenzhen, Guangdong, China; Departments of Neurology (Z.H., R.L., X.Z., J.L.) and Radiology (C.Z., H.Z.), Shenzhen Children's Hospital, Shenzhen, Guangdong, China; Department of Pediatric Neurology (Z.H.), Boston Children's Hospital, Boston, Massachusetts; and Research Department (Y. Zhou), Hong Kong Sanatorium and Hospital, Hong Kong, China.

Haifeng Wang, Zhanqi Hu, and Dian Jiang contributed equally to this work and share co-first authorship.

Some of the work was partially supported by the National Key R&D Program of China (2023YFB3811400), the Guangdong High-level Hospital Construction Fund (ynkt2021-zz11), the National Natural Science Foundation of Shenzhen Children's Hospital (ynkt2021-zz11), the Shenzhen Key Medical Discipline Construction Fund (SZXK033), the Shenzhen Fund for Guangdong Provincial High-Level Clinical Key Specialties (SZGSP012), the Sanming Project of Medicine in Shenzhen (SZSM201812005), the National Natural Science Foundation of China (62271474), the High-level Talent Program in Pearl River Talent Plan of Guangdong Province (2019QN01Y986) and the Shenzhen Science and Technology Program (KCCXF2021020163408012, KQTD20180413181834876 and JCYJ20210324115810030).

Please address correspondence to Jianxiang Liao, MD, Department of Neurology, Shenzhen Children's Hospital, Shenzhen, China; e-mail: liaojianxiang@vip.sina.com
<http://dx.doi.org/10.3174/ajnr.A8053>

biomarkers of drug-treatment outcomes for pediatric patients with epilepsy is an urgent need.

Currently, MR imaging provides excellent tissue contrast, which is a technique used routinely to diagnose TSC disease.¹³ Radiologists have difficulty distinguishing patients with pediatric refractory (resistant seizure) disease from those with seizure-controlled disease because these patients may have similar appearances in MR imaging. Recent artificial intelligence tools have been used to help radiologists assess the cortical tubers in rare pediatric TSC disease, including from MR images.¹⁴ Deep learning has promoted the progress of 3D volumetric classification.¹⁵⁻¹⁷ Previous studies have shown the ability of deep convolutional neural network (CNN) models to classify lung cancer and bone lesions on MR imaging with high accuracy.^{18,19} In addition, several studies have begun to combine images of multicontrast MR imaging, by using the complementary visual information from the multicontrast MR imaging to improve the performance of the classification.^{20,21} However, these studies required many images to train the CNNs, which were challenging to obtain in rare disorders like pediatric TSC disease. Until now, few studies have used deep learning methods to predict outcomes of drug treatment for epilepsy in rare pediatric TSC disease.

Because the quantity of patients with rare pediatric TSC is limited, some studies have only used some machine learning techniques for the prediction of epilepsy drug-treatment outcomes. For example, An et al²² predicted patients with drug-resistant epilepsy at the time of the first ASM prescription and achieved an area under curve (AUC) of 0.764 with random forests. However, their work mainly focused on patients with general epilepsy instead of pediatric patients with rare TSC. Recently, lesion location and type of information features of MR imaging have been identified to predict epilepsy drug-treatment outcomes in rare pediatric TSC disease with multilayer perceptron and achieved an AUC of 0.812.¹² However, the features of MR imaging were also typically extracted manually, possibly introducing errors, and the description of these features was usually qualitative, subjective, and nonspecific. With current state-of-the-art machine learning methods, it may be possible to achieve better performance in automated drug-treatment outcome prediction through analysis of advanced imaging. Until now, there are not any state-of-the-art machine learning methods that can achieve an AUC of approximately 0.90 to predict epilepsy drug-treatment outcomes in rare pediatric TSC applications. In this study, we aimed to develop a deep learning method for predicting the outcomes of epilepsy drug treatment in children with the rare TSC disease.

MATERIALS AND METHODS

Network Architectures of Imaging Data

Deep learning, especially CNNs, has been widely used in medical image processing.²³⁻²⁵ Among the different variants of CNNs, 2D Residual Network (ResNet: <https://keras.io/api/applications/resnet/>) has shown remarkable performance in image classification.²⁶ It is composed of residual blocks that are substantially deeper. In addition, the residual networks are easier to optimize and can gain accuracy from significantly increased depth. Additionally, although most imaging studies have used 2D CNNs as their model architecture, some studies have proposed 3D

CNNs that can fully use the spatial features of MR imaging and achieve better performance.²⁷⁻²⁹

Therefore, we have constructed a 3D CNN architecture based on the idea of ResNet,²⁶ which is a more developed model based on 2D-ResNet. The MR image-based models were the 3D version of the network modified on 2D-ResNet. ResNet3D models (<https://paperswithcode.com/lib/torchvision/resnet-3d>) were used for feature-extraction from imaging data. The ResNet3D classifying layer was replaced with an average pooling layer and a fully connected layer to perform the binary classification task. The neural network structure of ResNet3D is shown in Fig 1.

Network Architectures of Clinical Data

A fully connected neural network (FCNN) using clinical variables was separately developed for the classification task as in Table 1. FCNN consists of a series of fully connected layers of 1024, 512, 128, 64, 32, and 16 nodes with an interposing rectified linear unit (ReLU) activation and batch normalization layers. A final classification layer with a single node was used to perform the binary classification task of clinical variables.

Synthesis of T2WI and FLAIR

Cortical tubers and subcortical nodules are major brain manifestations of rare pediatric TSC disease. Improving the conspicuity of cortical tubers and subcortical nodules is very important for clinical radiologists to diagnose rare pediatric TSC disease.³⁰ T2WI provides higher lesion and brain contrast. However, there is a strong CSF signal in T2WI, which interferes with visualization of periventricular lesions. FLAIR images can suppress CSF. However, the lesion-brain contrast in FLAIR is not clear enough. No single sequence can generate all of the desired tissue-contrast features in 1 image due to the necessary trade-offs in the choice of MR imaging pulse sequence parameters. Recent work has shown that combining T2WI and FLAIR images can enhance the detection of MS lesions.^{31,32} However, methods to optimize combining T2WI and FLAIR in rare pediatric TSC disease have not been reported so far. Therefore, inspired by Wiggermann et al³¹ and Gabr et al,³² we propose to use FLAIR3 as a new synthetic technique to optimally combine T2WI and FLAIR in rare pediatric TSC disease as in the following equation,³²

$$\text{Equation 1} \quad \text{FLAIR3} = \text{FLAIR}^{1.55} \times \text{T2WI}^{1.45}.$$

This formula is used to balance the lesion and brain tissue contrast between T2WI and FLAIR images. Lesion-brain contrast levels were different in T2WI and FLAIR images, even at the same TE. Unlike T2WI, FLAIR introduces modest T1-weighting, which counteracts the effect of prolonged relaxation of T2 in the lesion, thereby reducing the lesion-to-brain contrast. In addition, only FLAIR produces CSF-nulled images. Therefore, combining the 2 images with optimized weights may yield the best lesion-to-brain contrast in patients with rare pediatric TSC.

Late Fusion Strategies

Recently, several studies³³⁻³⁵ reported that the late fusion model can most effectively grasp the data distribution and ultimately yielded the best prediction performances. Inspired from Eweje et al¹⁸ and Jonsson et al,²⁰ we developed a late fusion model to combine multiple sequences of MR imaging for a feature

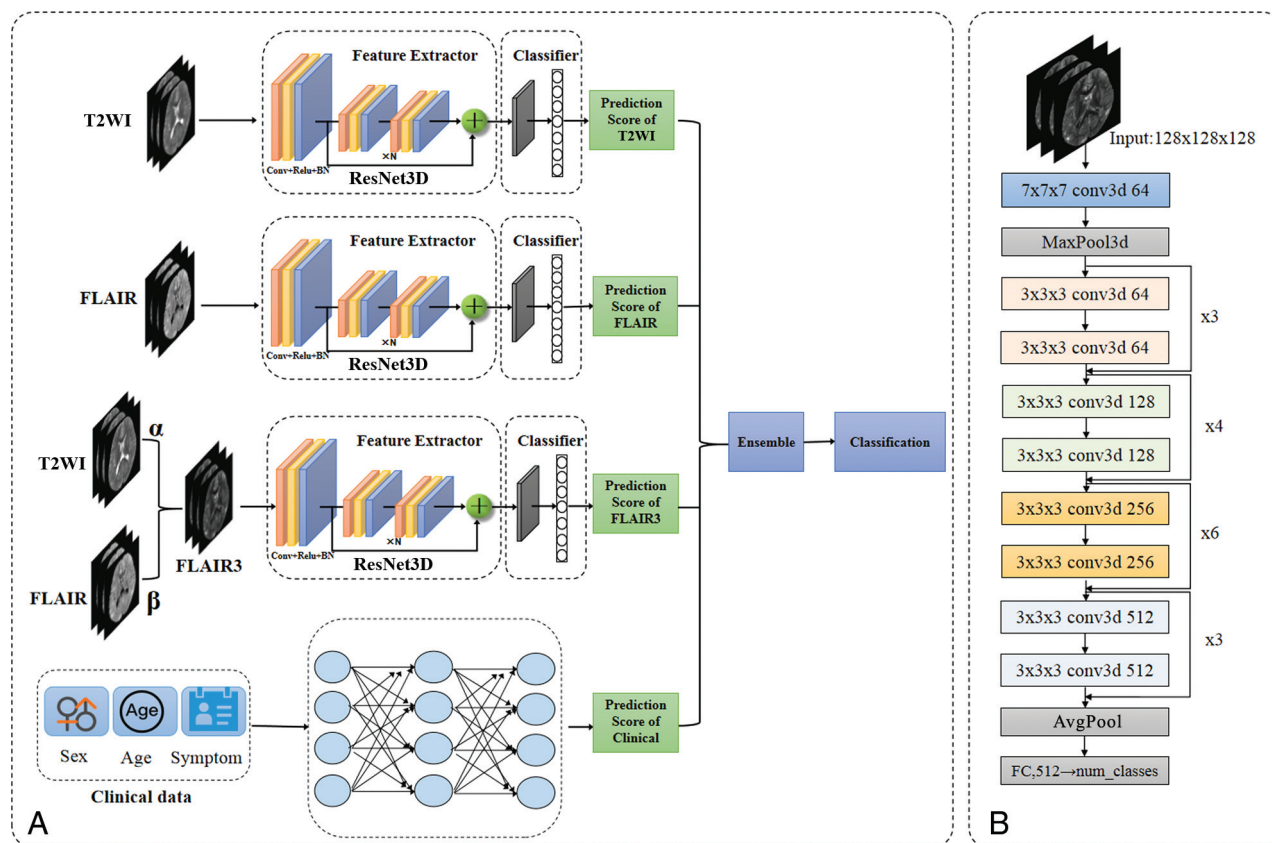


FIG 1. The net schematic of the proposed WAE-net method. *A*, Schematic of our proposed WAE-net pipeline. The ResNet3D took T2-weighted, FLAIR, and FLAIR3 images as input and output prediction scores, respectively. A FCNN model accepted age, sex, and TSC symptom variables as input and output a prediction score. A WAE-net used prediction scores from the T2-weighted, FLAIR, FLAIR3, and clinical models as input and output a final classification by a simple and effective direct weighted-averaging method. *B*, Network structure of ResNet3D. FC indicates fully connected layer; conv3d, 3D convolution.

Table 1: Network structure of FCNN using 1-dimensional clinical variables

Layer Name	Output Dims
Input layer	(1,4)
FC1	1024
FC2	512
FC3	128
FC4	64
FC5	32
FC6	16
Output layer	1

Note:—FC indicates fully connected layer; Dims, dimensions.

extractor. Then, clinical data were fed into an FCNN. The late fusion model used prediction scores from the T2WI, FLAIR, FLAIR3, and clinical models as input and output a final classification by a simple and effective weighted-average ensemble (WAE) method as follows,

$$WAE = W_1 \times T2WI + W_2 \times FLAIR$$

$$+ W_3 \times FLAIR3 + W_4 \times Clinical,$$

where $W_1 + W_2 + W_3 + W_4 = 1$. T2WI, FLAIR, FLAIR3 and Clinical represent the prediction scores of 3 input images and clinical data. WAE represents the output prediction scores W_1 , W_2 , W_3 , and W_4 are the weights of the prediction scores of the 4

input. The above multi-technique deep learning method is called as WAE-net, as shown in Fig 1.

For the pediatric TSC classification tasks with 1 single input image technique, 3D-ResNet34 architectures were applied. For the pediatric TSC classification tasks with 1 single-input clinical datum, FCNN architectures were applied. When WAE-net was used, 3 sequences of T2WI, FLAIR, FLAIR3 images, and clinical data were used as input. The late fusion model used prediction scores from the T2WI, FLAIR, FLAIR3, and the clinical model as input and output a final classification by a simple and effective weighted-average method. In our experiments, W_1 , W_2 , W_3 and W_4 , which were the weights of the prediction scores of the 4 inputs, are the same.

Participant Data

In this study, all pediatric patients came from Shenzhen Children's Hospital between January 2013 and September 2021, diagnosed with rare TSC-related epilepsy. Three hundred pediatric patients with ASM treatment for at least 1 year were enrolled in the retrospective study. Written informed consent was obtained from all subjects before the study, and the protocols and study were approved by the institutional review board of the Shenzhen Children's Hospital. Written informed consent was obtained from patients with rare TSC and/or their parents. All MR imaging scans included FLAIR images and T2WI before ASM treatment.

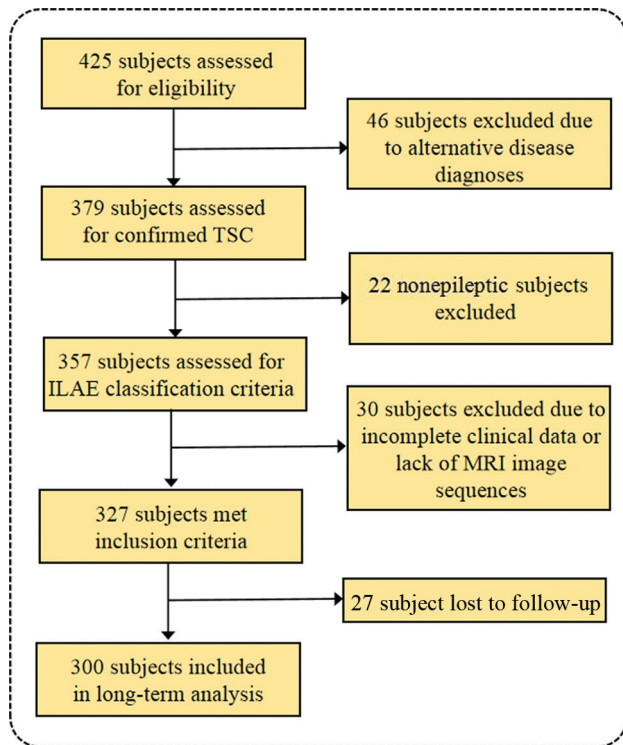


FIG 2. Study inclusion criteria. Flow chart details the identification of the study cohort. ILAE indicates International League Against Epilepsy.

Otherwise, drug-treatment outcomes were defined according to the 1981 International League Against Epilepsy classification,³⁶ which were recorded as a controlled group or an uncontrolled group. Pediatric patients were considered as the controlled group if they did not have clinical seizures for at least 1 year. Uncontrolled pediatric patients (refractory patients) had at least 1 seizure in the past year. Figure 2 shows the inclusion criteria.

Imaging Data

Binary classification models were trained to distinguish pediatric uncontrolled seizures from controlled seizures on T2-weighted, FLAIR, and FLAIR3 images. Five-fold cross-validation was used to evaluate the models. Using the ResNet3D architecture,³⁷ models were trained with a learning rate of 0.001, batch size of 4 for 100 epochs, Adam optimization (https://www.researchgate.net/publication/352497171_Adam_Optimization_Algorithm), and the loss function of focal loss. The area under the receiver operating characteristic (ROC) of cross-validation (AUC) as the metric for model evaluation, while preserving the model, achieved the best level of AUC during training. After training, we used the parameters of all 5 models, which originated from 5-fold cross-validation, to test. The prediction score of each pediatric patient was determined by the average of the prediction scores of the 5 models from 5-fold cross-validation. Figure 3B shows the training and evaluation scheme.

Pediatric data were randomly split into a training and validation data set ($n=240$) and an independent test data set ($n=60$). We trained all the models using an NVIDIA RTX A6000 GPU card (<https://www.techpowerup.com/gpu-specs/rtx-a6000.c3686>). Training, validation, and test of models were implemented with Python (Version 3.8.10) and PyTorch (Version 1.9.0) environments.

T2WI was registered into the FLAIR space using the FMRIB Linear Image Registration Tool (FLIRT; <http://www.fmrib.ox.ac.uk/fsl/wiki/FLIRT>) of FSL, which used mutual information as the cost function.³⁸ In neuroimaging studies, most lesions were located in the brain tissue. Therefore, we first used the deep learning tool HD-bet (<https://bio.tools/HD-BET#!>)³⁹ to dissect the skull in MR imaging.

The 3D MR images were resized to 128, 128, 128, and the image intensity was then normalized to the range between 0 and 1, using Equation 2 as follows,

$$\text{Equation 3} \quad \text{Normalized}(x) = \frac{x - \text{Min}(x)}{\text{Max}(x) - \text{Min}(x)},$$

where $\text{Max}(x)$ and $\text{Min}(x)$ are the maximum and minimum of the brain-extracted MR images and $\text{Normalized}(x)$ is the normalized MR images. Finally, T2WI and FLAIR were combined into FLAIR3. Figure 3A shows the schematic of the data-preprocessing pipeline.

Clinical Data

The FCNN model for clinical feature-based classification was also trained with a learning rate of 0.001, batch size of 4 for 100 epochs, Adam optimization, and the loss function of focal loss. Five-fold cross-validation was used to evaluate the models. The clinical features with statistical significance ($P < .05$) were selected as the final feature input of the FCNN model.

Evaluation Model

Here, AUC, accuracy (ACC), sensitivity (SEN), and specificity (SPE) were calculated to assess the classification performance for each model in each cohort. These metrics are defined in terms of true-positive (TP), which is the total number of positive classifications that are correct; true-negative (TN), which is the total number of negative classifications that are correct; false-positive (FP), which is the total number of positive classifications that are incorrect, and false-negative (FN) which is the total number of negative classifications that are incorrect. ACC, SEN, and SPE are calculated by using the following equations:

ACC: The percentage of the whole sample that is correctly classified.

$$\text{Equation 4} \quad \text{ACC} = \frac{TP + TN}{TP + TN + FP + FN}.$$

SEN: The percentage of the total sample that is true that is correctly classified.

$$\text{Equation 5} \quad \text{SEN} = \frac{TP}{TP + FN}.$$

SPE: The percentage of the total sample that is negative and correctly classified.

$$\text{Equation 6} \quad \text{SPE} = \frac{TN}{TN + FP}.$$

Statistical Analysis

Here, we used frequencies and percentages for categoric variables and mean (SD) for continuous variables. To compare pairs of groups, we used F -tests for continuous variables and χ^2 tests for categoric variables. $P < .05$ was defined as significant. All statistical

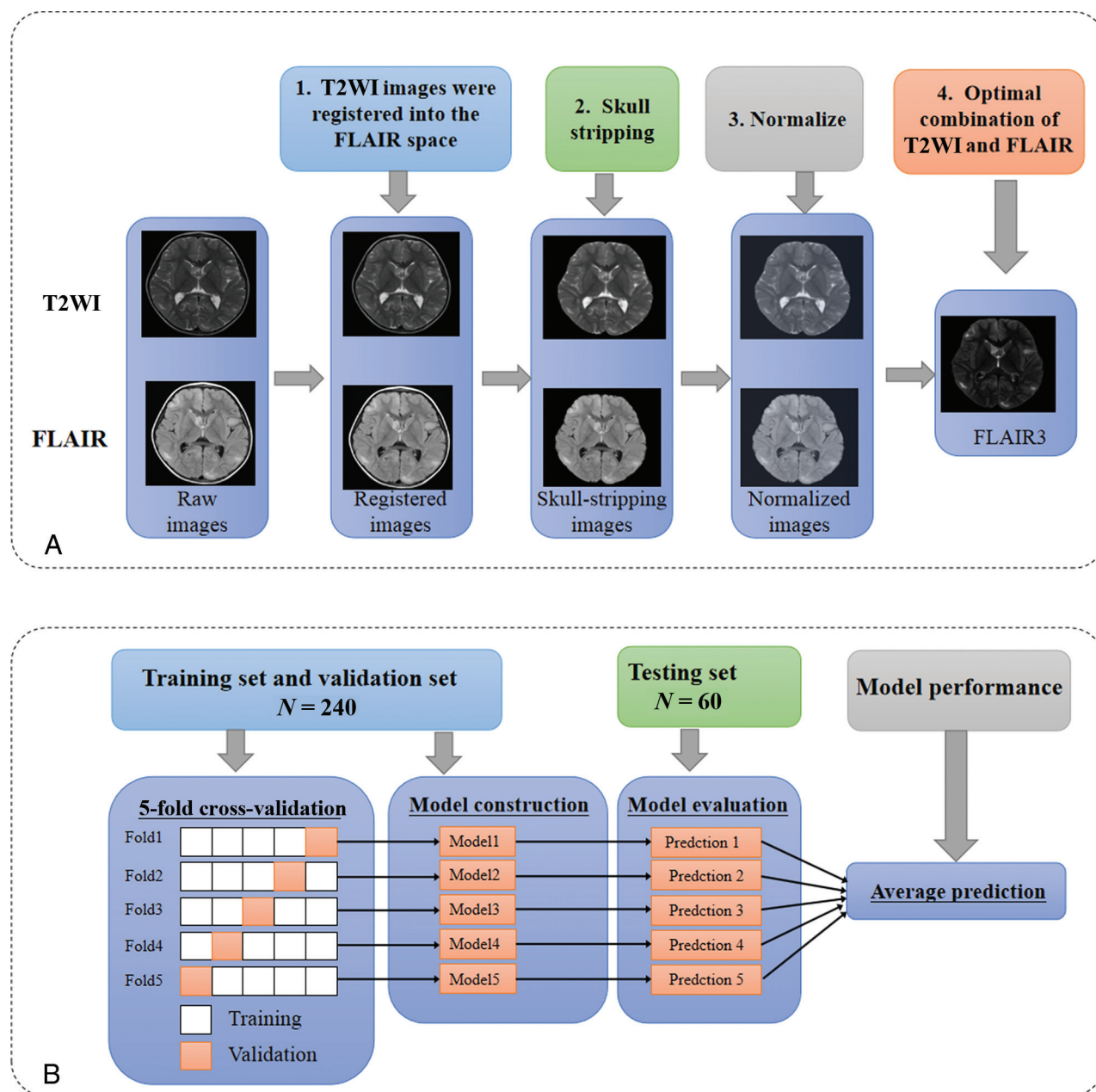


FIG 3. The applied operations of preprocessing pipeline, training, and evaluation. Schematic of the data preprocessing pipeline (A) and training and evaluation scheme (B). Five models were trained for each technique and used to predict drug-treatment outcome individually. The 5 predictions were averaged to give the final prediction of the model performances.

Table 2: The clinical characteristics of pediatric patients with rare TSC^a

Characteristics	Controlled (n = 97)	Uncontrolled (n = 203)	P Value
Male (No.) (%)	56 (57.7%)	107 (52.7%)	.416
Age at onset (mean) (months)	30.44 (SD, 33.17)	17.35 (SD, 26.22)	<.001 ^b
Age at imaging (mean) (months)	57.01 (SD, 45.18)	36.27 (SD, 40.37)	<.001 ^b
Infantile spasms (No.) (%)	21 (21.6%)	93 (45.8%)	<.001 ^b
Epilepsy (No.) (%)	97 (100.0%)	203 (100.0%)	
ASM numbers (≥3), n (%)	42 (43.3%)	171 (84.2%)	<.001 ^b
Focal epilepsy (No.) (%)	75 (77.3%)	165 (81.3%)	.424

Note:—Controlled indicates controlled seizures; Uncontrolled, uncontrolled seizures.

^a P values of continuous variables are the results of F-tests, and P values of categorical variables are the results of χ^2 tests.

^b The statistical significance between the groups.

analyses were performed using scikit-learn (<https://scikit-learn.org/stable/index.html>), scipy (<https://scipy.org/>), and stats (<https://pypi.org/project/statsmodels/>) models in Python 3.8.10.

RESULTS

Patient Characteristics

The main patient characteristics of all 300 patients with rare pediatric TSC-related disease are listed in Table 2. Of

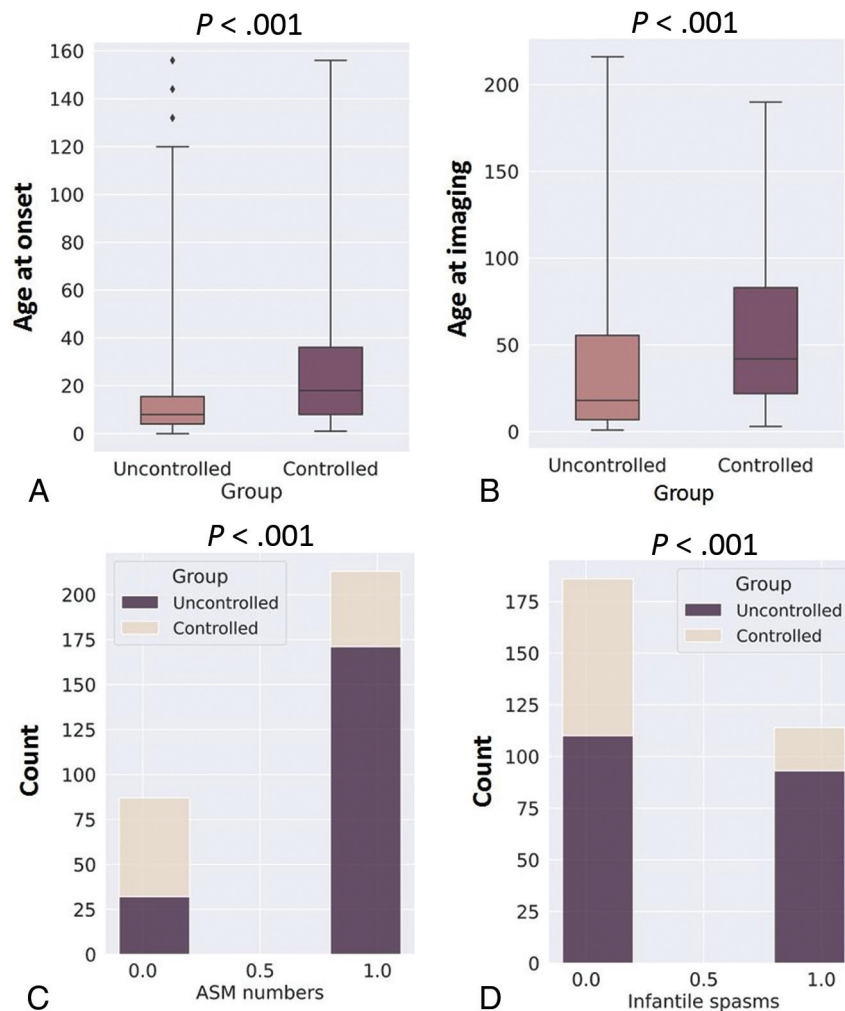


FIG 4. Statistical analysis of the clinical data set. A and B, Boxplots for continuous variables. A, Age at onset. B, Age at imaging. The horizontal axis represents groups, and the vertical axis represents features. The middle line of the boxplot is the median of the feature data. The upper and lower bounds of the boxplot are the upper and lower quartiles of the feature data, respectively. P values are the results of the Spearman correlation test. C and D, Stacked barplots for categorical variables. C, Infantile spasms. D, ASM numbers (≥ 3). The horizontal axis represents features (1.0 represents ASM numbers ≥ 3 or infantile spasms; 0.0 represents ASM numbers < 3 or no infantile spasms), and the vertical axis represents the number of patients in the 2 groups. P values of continuous variables are the results of F-tests, and P values of categorical variables are the results of χ^2 tests.

the 300 enrolled patients, 97 (41.1%) were controlled and 203 (58.9%) were uncontrolled by drug treatment. Thirty-one (41.3%) and 8 (40.0%) patients had controlled seizures, while 44 (58.7%) and 12 (60.0%) patients had uncontrolled seizures in the training and test cohorts, respectively. Of the 300 patients with TSC, 56 (57.7%) were male in the controlled seizures group and 107 (52.7%) were male in the uncontrolled group. The ages at onset in children with rare TSC were 30.44 (SD, 33.17) months and 17.35 (SD, 26.22) months in the controlled and uncontrolled groups, respectively. The ages at imaging of the children with TSC were 57.01 (SD, 45.18) months and 36.27 (SD, 40.37) months in the controlled and uncontrolled groups, respectively. There were no significant differences between the 2 drug-treatment outcomes based on sex and focal epilepsy features ($P > .05$). Age of onset, age at imaging, infantile spasms, and ASM numbers were significantly different between the 2 drug-treatment outcomes ($P < .05$).

Boxplots for age of onset and age at imaging and stacked barplots for infantile spasms and ASM numbers are shown in Fig 4. From the figure, we can see that the number of patients with

infantile spasms in the uncontrolled group was much larger than that in the controlled group. The number of pediatric patients with ASM numbers of 3 in the uncontrolled group was much higher than that in the controlled group.

Synthetic FLAIR3

Figure 5 shows FLAIR, T2WI, and synthetic FLAIR3 images in a representative child with rare TSC in the controlled group and a child with rare TSC in the uncontrolled group and a healthy child. Note the improved lesion contrast and visibility of the lesions on the synthetic FLAIR3 images of the child with rare TSC. The TSC lesion is shown by the white arrow.

Model Performance

The performance results compared with other networks on FLAIR is shown in Table 3. When the network inputs are FLAIR, ResNet3D achieved the best AUC performance. Performance of the final T2-weighted, FLAIR, FLAIR3, clinical data, and proposed WAE-net models on the test set are described in Table 4 and Fig 6.

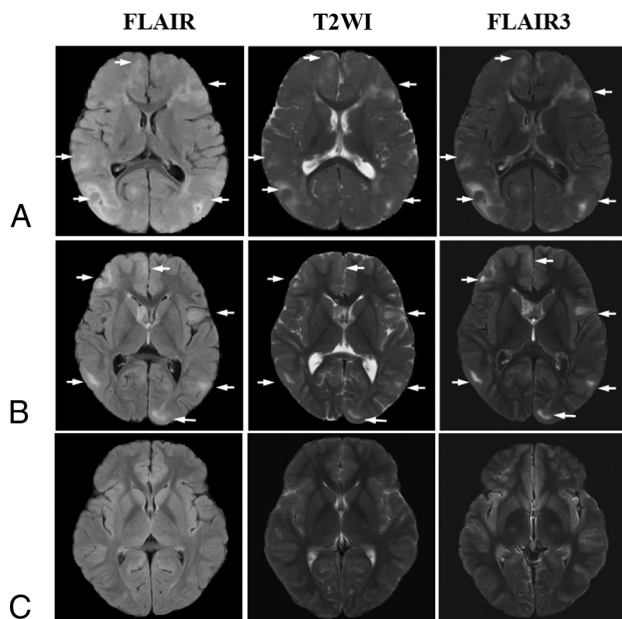


FIG 5. Representative images from a child with TSC in the controlled group, a child with TSC in the uncontrolled group, and a healthy child shown on T2WI, FLAIR, and the proposed synthetic FLAIR3 (TSC lesion, white arrow). Controlled group (A) uncontrolled group (B), and healthy child group (C).

Table 3: Performance results compared with other networks on FLAIR

Technique	Model	AUC	ACC	SEN	SPE
FLAIR	ResNet3D	0.783	0.695	0.650	0.790
FLAIR	LeNet3D	0.660	0.644	0.600	0.737
FLAIR	VGG3D	0.765	0.746	0.825	0.579

Note:—ResNet3D is derived from He et al;²⁶ LeNet3D is derived from Simonyan;⁴⁶ VGG3D is derived from Szegedy et al.⁴⁷

Table 4: The results of testing set

Technique	Model	AUC	ACC	SEN	SPE
FLAIR	ResNet3D	0.783	0.695	0.650	0.790
T2WI	ResNet3D	0.649	0.593	0.450	0.895
FLAIR3	ResNet3D	0.730	0.695	0.700	0.684
Clinical data	FCNN	0.774	0.831	0.950	0.579
FLAIR+ clinical data	WAE-net	0.826	0.847	0.974	0.580
FLAIR3+ clinical data	WAE-net	0.887	0.831	0.850	0.789
T2WI+ clinical data	WAE-net	0.809	0.847	0.975	0.579
Ensemble all	WAE-net	0.908	0.847	0.850	0.842

The clinical pediatric data-based model results were trained using age of onset, age at imaging, infantile spasms, and ASM numbers with an AUC of 0.774, ACC of 0.831, SEN of 0.950, and SPE of 0.579 in the testing cohort. The AUC performance of FLAIR3 was better than that of T2WI using the same network. When both FLAIR3 and clinical data are fed into the network, the network achieves an AUC performance of 0.887, which is higher than the AUC performance of T2-weighted data plus clinical data and FLAIR data plus clinical pediatric data. When T2-weighted (T2W), FLAIR, FLAIR3, and clinical pediatric data are all ensemble to input into the proposed network ('Ensemble all' in Table 4 and Fig 6), the best classification results were obtained for the proposed WAE-net model with an AUC of 0.908, ACC of 0.847, SEN

of 0.850, and SPE of 0.842 in the testing cohort. Figure 7A, -B shows the ROC curve for T2-weighted, FLAIR, FLAIR3, clinical pediatric data, and the performance of the proposed WAE-net models on the test set. Figure 7C, -D shows the decision curve analysis (DCA) for T2-weighted, FLAIR, FLAIR3, clinical pediatric data, and the performance of the proposed WAE-net models on the test set.

DISCUSSION

Reliable prediction of epilepsy drug-treatment outcomes allows more targeted treatment and can improve cure rates and may protect neurodevelopment.^{4,8,40} However, it is difficult for clinicians to determine epilepsy drug-treatment outcomes on the basis of clinical and treatment presentation. Therefore, there is an urgent need to develop a pediatric model that can predict epilepsy drug-treatment outcomes before treatment initiation.

Therefore, for the first time, we have developed a deep learning model to predict the drug-treatment outcome and have first introduced FLAIR3 as a new technique into the rare pediatric TSC diagnosis to improve lesion contrast. Our approach uses a deep neural network framework to extract descriptive factors from multicontrast MR images and clinical pediatric data. The proposed WAE-net model achieved the best AUC performance of 0.908 in the testing cohort when T2-weighted, FLAIR, FLAIR3, and clinical data are all input to the network. The structural MR images were complemented by demographic information (age at onset and age at imaging) and infantile spasms and ASM numbers collected at the baseline visit to compute a combined score used to predict epilepsy drug-treatment outcome. Compared with the single technique with ResNet3D approaches, the proposed WAE-net can improve the pediatric classification performance, meaning that combining multiple-contrast MR imaging and clinical pediatric data can use the complementary information between the two.^{20,21} Moreover, ResNet, with extremely high accuracies in the ImageNet data set (<https://image-net.org/>) has rapidly become a good choice for image-recognition tasks.²⁶ However, to the best of our knowledge, this article is the first to consider the ResNet3D of CNN architectures for diagnosis in rare pediatric TSC disease.

We specifically selected these structural MR imaging and clinical pediatric data to create a classification method that used the least invasive, lowest cost, and more commonly used diagnostic tools in clinical applications. In other words, the MR imaging and clinical pediatric data that we included here can typically be collected in nontertiary or highly specialized medical centers, greatly increasing the potential applicability of our method in clinical pediatric practice. For example, we did not use PET and fMRI as biomarkers because these imaging data are more expensive and less diffuse than the MR imaging and clinical pediatric data used here. In addition, a significant advantage of MR imaging over other imaging modalities such as CT and nuclear imaging is that it clearly shows soft tissues in multicontrasts.⁴¹

In addition, we found that FLAIR3 could improve lesion contrast and visibility of the lesions and that the AUC performance of FLAIR3 is better than that of T2WI by using the same neural network. In addition, the AUC performance of FLAIR3 data plus clinical data is higher than the AUC performance of T2-weighted

Performances of All Models

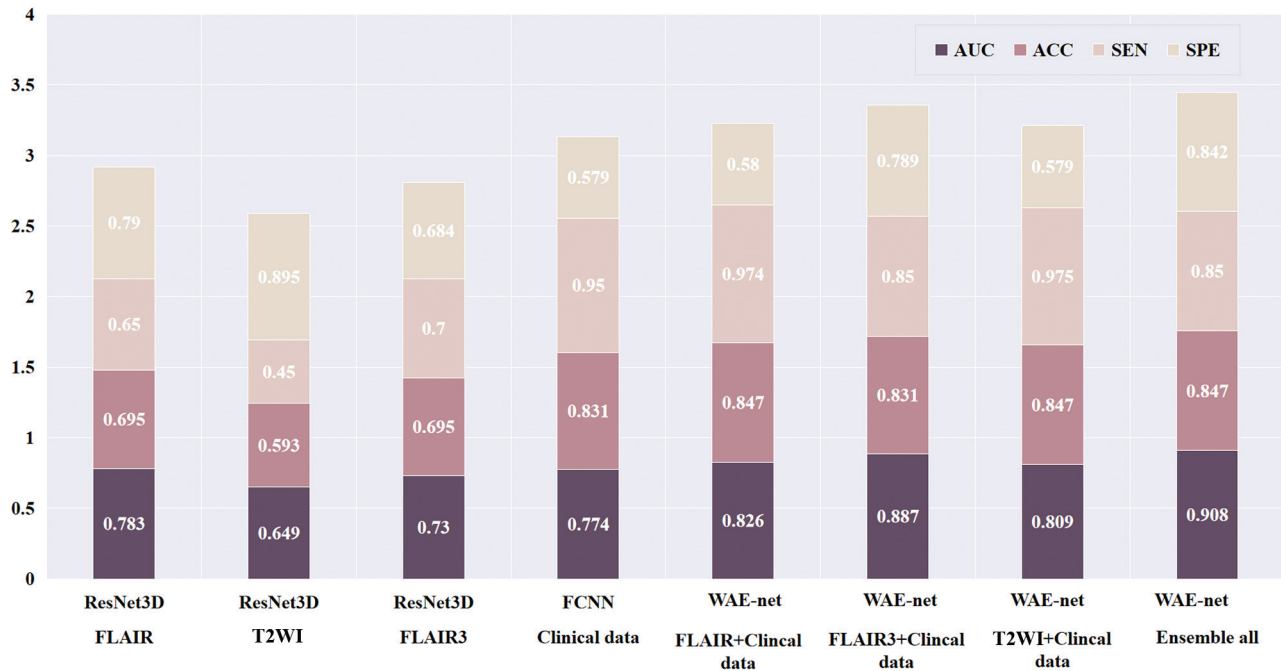


FIG 6. The performances of the final T2-weighted, FLAIR, FLAIR3, clinical pediatric data, and the proposed WAE-net models on the test set.

data plus clinical pediatric data and FLAIR data plus clinical pediatric data. One possible explanation is that FLAIR3 can improve the lesion-to-brain contrast and provide more low-dimensional visual lesion information for a rare pediatric TSC diagnosis, which may increase the interpretability of deep learning and support the idea that deep learning methods can identify the more relevant features from the input images.⁴² Previous studies⁴³⁻⁴⁵ have identified several risk factors affecting epilepsy prognosis in pediatric patients with TSC, including the age of onset of seizures, the presence of infantile spasm, and a history of using >3 antiepileptic drugs. In our study, we also observed the impact of age at onset and age at imaging on the prognosis of epilepsy. Specifically, we found that these factors were statistically different between the controlled and uncontrolled groups ($P < .05$), with the uncontrolled group being younger. Our findings suggest that pediatric patients with a younger age of onset and imaging are more likely to have a poorer prognosis. Pediatric patients with focal seizures before 1 year of age are more likely to develop resistance than patients with onset after 1 year of age.³ Jeong et al⁴⁵ also reported that pediatric patients with rare TSC epilepsy with previous infantile spasms are more likely to have drug resistance,³ which is consistent with our conclusion that the uncontrolled group has a higher proportion of infantile spasms.

In our study, we included pediatric patients with confirmed rare TSC-related epilepsy in Shenzhen Children's Hospital for 8 years, followed the patients for >1 year, and finally included 300 children with rare TSC-related epilepsy. During the experiments, we found that the proposed 3D CNN models can achieve better performance than the traditional machine learning approach from Yang et al.¹² They achieved an AUC of 0.812 with multilayer perceptron.¹² However, this study also had small sample sizes. We

did not find any studies involving deep learning techniques for the prediction of epilepsy drug-treatment outcome on MR imaging. Intuitively, neural network-based methods should perform better than conventional approaches for feature-extraction followed by a separate classifier, because the feature-selection process is directly driven by the performance-optimization procedures.¹⁶ Deep learning is required for a number of training samples to achieve good generalization performance. We believe the performance improvement of our method is primarily caused by fully using the spatial features of 3D MR imaging and complementary information of clinical pediatric data. The increase in the number of pediatric data sets may also be 1 reason.

The rarity of TSC presents a challenge in compiling a data set that could effectively power the training of a deep neural network for this task. Although the size of our data set is larger than that of many other data sets used for rare disease classification tasks, it is still orders of magnitude smaller than data sets used for other medical image characterization tasks. Larger data sets could also allow granular classification beyond binary, such as distinguishing infantile spasms or other histopathologic diagnoses.

Several limitations should be noted for the current pediatric study. First, we conducted this study in a retrospective manner without external validation, having the risk of bias and lack of generalizability. Second, the study participants belonged to a single ethnicity (Chinese), implying that our results might not be applicable to pediatric patients from other ethnic backgrounds. Collecting multicenter data sets is challenging due to the extremely low incidence of rare pediatric TSC disease and the need to follow pediatric patients with rare TSC for ≥ 1 year. Future prospective studies that incorporate data from other international centers and larger data samples can overcome this limitation.

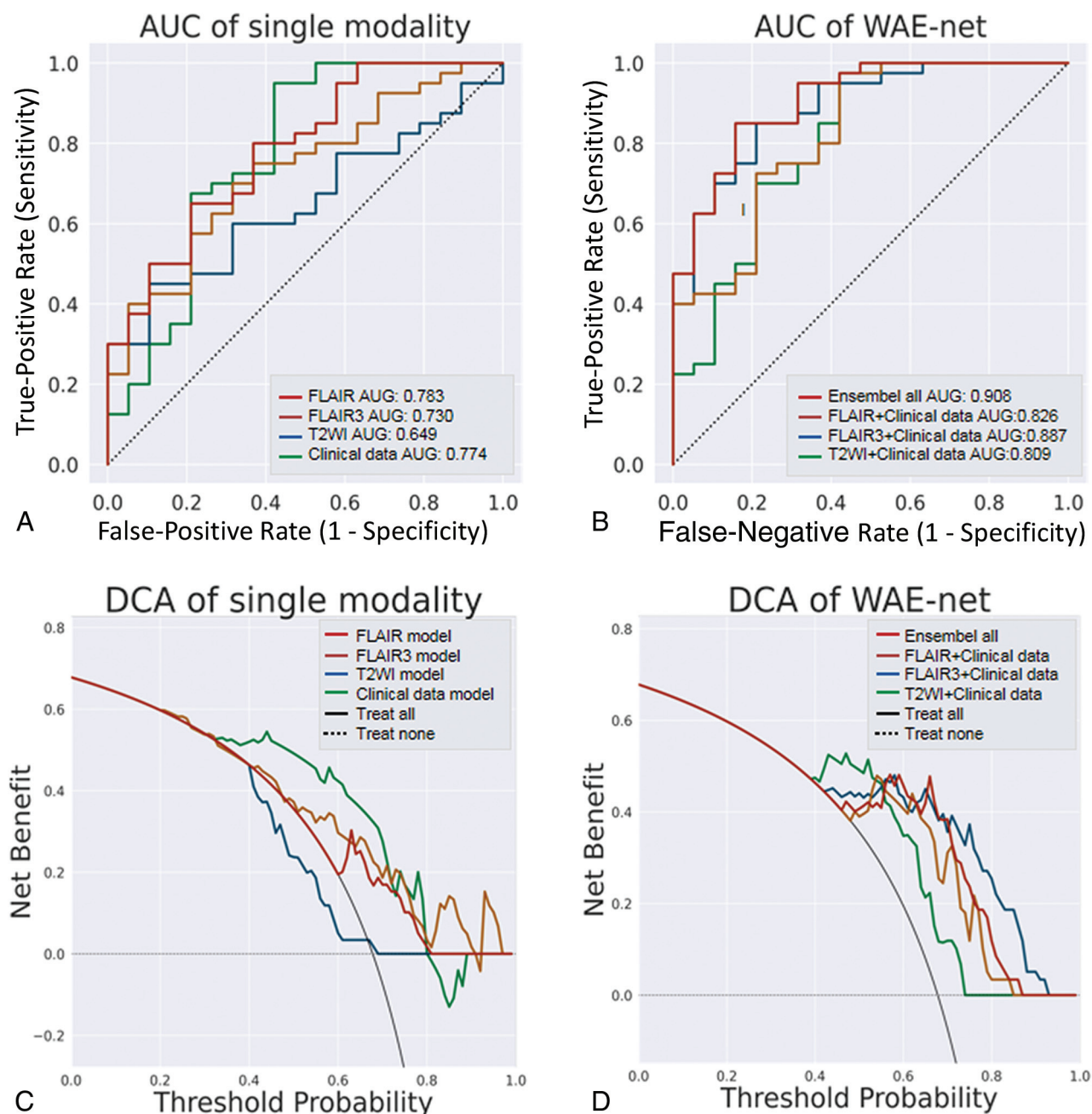


FIG 7. Analysis of the single technique and the proposed WAE-net methods. *A*, ROC curves in FLAIR, T2-weighted, FLAIR3, and the clinical model of the testing cohort. *B*, ROC curves in the proposed WAE-net of the testing cohort. *C*, DCA for FLAIR decision. T2-weighted, FLAIR3, and the clinical model of the testing cohort. *D*, DCA for the proposed WAE-net of the testing cohort. The *black line* represents the assumption that all patients have interventions. The *black dotted line* represents the assumption that no patients have interventions. The *colored lines* represent the different models. The *horizontal axis* represents the threshold probability, and the *vertical axis* represents the net benefit.

In short, for the first time, we introduce FLAIR3 as a new technique in the rare pediatric TSC diagnosis to improve lesion contrast, and we have developed a deep learning model that can predict epilepsy drug-treatment outcomes with high AUC and accuracy. At present, this work demonstrates the promise of deep learning to aid radiologists in characterizing the refractory patients with improved certainty. FLAIR3 can provide clinicians with a new technique to accurately localize lesions in patients with rare pediatric TSC.

CONCLUSIONS

In general, age of onset, age at imaging, infantile spasms, and ASM numbers were shown to be related to epilepsy drug-treatment outcome in children with rare TSC. FLAIR3 can improve lesion contrast and visibility and provide more complementary information for our deep learning models to improve the prediction accuracy. The experiments have shown that the proposed deep learning method could successfully predict epilepsy drug-treatment outcomes in children with rare TSC-related disease.

The current test results have suggested that the proposed method could be a noninvasive, efficient, and reliable way to predict pediatric TSC-related drug-treatment outcomes and could be as a strong baseline for future pediatric researchers.

Disclosure forms provided by the authors are available with the full text and PDF of this article at www.ajnr.org.

REFERENCES

- Randle SC. **Tuberous sclerosis complex: a review.** *Pediatr Ann* 2017;46:e166–171 [CrossRef Medline](#)
- Holmes GL, Stafstrom CE; Tuberous Sclerosis Study Group. **Tuberous sclerosis complex and epilepsy: recent developments and future challenges.** *Epilepsia* 2007;48:617–30 [CrossRef Medline](#)
- Chu-Shore CJ, Major P, Camposano S, et al. **The natural history of epilepsy in tuberous sclerosis complex.** *Epilepsia* 2010;51:1236–41 [CrossRef Medline](#)
- Ślowińska M, Jóźwiak S, Peron A, et al. **Early diagnosis of tuberous sclerosis complex: a race against time—how to make the diagnosis before seizures?** *Orphanet J Rare Dis* 2018;13:25 [CrossRef Medline](#)
- Henske EP, Jóźwiak S, Kingswood JC, et al. **Tuberous sclerosis complex.** *Nat Rev Dis Primers* 2016;2:16035 [CrossRef Medline](#)
- Strzelczyk A, Rosenow F, Zollner JP, et al. **Epidemiology, healthcare resource use, and mortality in patients with tuberous sclerosis complex: a population-based study on German health insurance data.** *Seizure* 2021;91:287–95 [CrossRef Medline](#)
- Jansen FE, van Huffelen AC, Bourez-Swart M, et al. **Consistent localization of interictal epileptiform activity on EEGs of patients with tuberous sclerosis complex.** *Epilepsia* 2005;46:415–19 [CrossRef Medline](#)
- Curatolo P, Nabbout R, Lagae L, et al. **Management of epilepsy associated with tuberous sclerosis complex: updated clinical recommendations.** *Eur J Paediatr Neurol* 2018;22:738–48 [CrossRef Medline](#)
- van der Poest Clement E, Jansen FE, Braun KP, et al. **Update on drug management of refractory epilepsy in tuberous sclerosis complex.** *Paediatr Drugs* 2020;22:73–84 [CrossRef Medline](#)
- Jesmanas S, Norvainytė K, Gleiznienė R, et al. **Different MRI-defined tuber types in tuberous sclerosis complex: quantitative evaluation and association with disease manifestations.** *Brain Dev* 2018;40:196–204 [CrossRef Medline](#)
- Tong XZ, Wang XF, Qin L, et al. **Vagus nerve stimulation for drug-resistant epilepsy induced by tuberous sclerosis complex.** *Epilepsy Behav* 2022;126:108431 [CrossRef Medline](#)
- Yang J, Zhao C, Su S, et al. **Machine Learning in Epilepsy Drug Treatment Outcome Prediction Using Multi-modality Data in Children with Tuberous Sclerosis Complex.** In: *2020 6th International Conference on Big Data and Information Analytics (BigDIA)*. December 4–6, 2020. Shenzhen, China [CrossRef](#)
- Russo C, Nastro A, Cicala D, et al. **Neuroimaging in tuberous sclerosis complex.** *Childs Nerv Syst* 2020;36:2497–509 [CrossRef Medline](#)
- Sanchez Fernandez I, Yang E, Calvachi P, et al; TACERN Study Group. **Deep learning in rare disease: detection of tubers in tuberous sclerosis complex.** *PLoS One* 2020;15:e0232376 [CrossRef Medline](#)
- Hu J, Qing Z, Liu R, et al. **Deep learning-based classification and voxel-based visualization of frontotemporal dementia and Alzheimer's disease.** *Front Neurosci* 2020;14:626154 [CrossRef Medline](#)
- Spasov S, Passamonti L, Duggento A, et al; Alzheimer's Disease Neuroimaging Initiative. **A parameter-efficient deep learning approach to predict conversion from mild cognitive impairment to Alzheimer's disease.** *Neuroimage* 2019;189:276–87 [CrossRef Medline](#)
- Kim H, Lee Y, Kim YH, et al. **Deep learning-based method to differentiate neuromyelitis optica spectrum disorder from multiple sclerosis.** *Front Neurol* 2020;11:599042 [CrossRef Medline](#)
- Eweje FR, Bao B, Wu J, et al. **Deep learning for classification of bone lesions on routine MRI.** *EBioMedicine* 2021;68:103402 [CrossRef Medline](#)
- Grossman R, Haim O, Abramov S, et al. **Differentiating small-cell lung cancer from non-small-cell lung cancer brain metastases based on MRI using efficientnet and transfer learning approach.** *Technol Cancer Res Treat* 2021;20:153303382110049 [CrossRef Medline](#)
- Jonsson BA, Bjornsdottir G, Thorgeirsson TE, et al. **Brain age prediction using deep learning uncovers associated sequence variants.** *Nat Commun* 2019;10:5409 [CrossRef Medline](#)
- Peng H, Gong W, Beckmann CF, et al. **Accurate brain age prediction with lightweight deep neural networks.** *Med Image Anal* 2021;68:101871 [CrossRef Medline](#)
- An S, Malhotra K, Dilley C, et al. **Predicting drug-resistant epilepsy: a machine learning approach based on administrative claims data.** *Epilepsy Behav* 2018;89:118–25 [CrossRef Medline](#)
- Lockett PH, Maccotta L, Lee JJ, et al. **Deep learning resting state fMRI lateralization of temporal lobe epilepsy.** *Epilepsia* 2022;63:1542–52 [CrossRef Medline](#)
- Gleichgerricht E, Munsell B, Bhatia S, et al. **Deep learning applied to whole-brain connectome to determine seizure control after epilepsy surgery.** *Epilepsia* 2018;59:1643–54 [CrossRef Medline](#)
- Zhang Q, He Y, Qu T, et al. **Delayed brain development of Rolandic epilepsy profiled by deep learning-based neuroanatomic imaging.** *Eur Radiol* 2021;31:9628–37 [CrossRef Medline](#)
- He K, Zhang X, Ren S, et al. **Deep residual learning for image recognition.** In: *Proceedings of the IEEE Conference on Computer Vision and Pattern Recognition*. June 27–30, 2016. Las Vegas, Nevada
- Cole JH, Poudel RP, Tsagkrasoulis D, et al. **Predicting brain age with deep learning from raw imaging data results in a reliable and heritable biomarker.** *Neuroimage* 2017;163:115–24 [CrossRef Medline](#)
- Meyer A, Chlebus G, Rak M, et al. **Anisotropic 3D multi-stream CNN for accurate prostate segmentation from multi-planar MRI.** *Comput Methods Programs Biomed* 2021;200:105821 [CrossRef Medline](#)
- Folego G, Weiler M, Casseb RF, et al. **Alzheimer's disease detection through whole-brain 3D-CNN MRI.** *Front Bioeng Biotechnol* 2020;8:534592 [CrossRef Medline](#)
- Grilli G, Moffa AP, Perfetto F, et al. **Neuroimaging features of tuberous sclerosis complex and Chiari type I malformation: a rare association.** *J Paediatr Neurosci* 2018;13:224–28 [CrossRef Medline](#)
- Wiggermann V, Hernandez-Torres E, Traboulsee A, et al. **FLAIR2: a combination of FLAIR and T2 for improved MS lesion detection.** *AJNR Am J Neuroradiol* 2016;37:259–65 [CrossRef Medline](#)
- Gabr RE, Hasan KM, Haque ME, et al. **Optimal combination of FLAIR and T2-weighted MRI for improved lesion contrast in multiple sclerosis.** *J Magn Reson Imaging* 2016;44:1293–300 [CrossRef Medline](#)
- Liang G, Xing X, Liu L, et al. **Alzheimer's disease classification using 2D convolutional neural networks.** *Annu Int Conf IEEE Eng Med Biol Soc* 2021;2021:3008–12 [CrossRef Medline](#)
- Jiang D, Liao J, Zhao C, et al. **Recognizing pediatric tuberous sclerosis complex based on multi-contrast MRI and deep weighted fusion network.** *Bioengineering (Basel)* 2023;10:870 [CrossRef Medline](#)
- Hu Z, Jiang D, Zhao X, et al. **Predicting drug treatment outcomes in children with tuberous sclerosis complex-related epilepsy: a clinical radiomics study.** *AJNR Am J Neuroradiol* 2023;44:853–60 [CrossRef Medline](#)
- Shinnar S. **The new ILAE classification.** *Epilepsia* 2010;51:715–17 [CrossRef Medline](#)
- Tan M, Efficientnet LQ. **Rethinking model scaling for convolutional neural networks.** In: *Thirty-Sixth International Conference on Machine Learning*. June 9–15, 2019. Long Beach, California
- Jenkinson M, Beckmann CF, Behrens TE, et al. **FSL.** *Neuroimage* 2012;62:782–90 [CrossRef Medline](#)
- Isensee F, Schell M, Pflueger I, et al. **Automated brain extraction of multisequence MRI using artificial neural networks.** *Hum Brain Mapp* 2019;40:4952–64 [CrossRef Medline](#)
- Hsieh DT, Jennesson MM, Thiele EA. **Epileptic spasms in tuberous sclerosis complex.** *Epilepsy Res* 2013;106:200–10 [CrossRef Medline](#)
- Lyu Q, Shan H, Steber C, et al. **Multi-contrast super-resolution MRI through a progressive network.** *IEEE Trans Med Imaging* 2020;39:2738–49 [CrossRef Medline](#)
- Jaworek-Korjakowska J, Brodzicki A, Cassidy B, et al. **Interpretability of a deep learning based approach for the classification of skin**

- lesions into main anatomic body sites. *Cancers (Basel)* 2021;13:6048 [CrossRef Medline](#)
43. Gül Mert G, Altunbaşak Ş, Hergüner Ö, et al. **Factors affecting epilepsy prognosis in patients with tuberous sclerosis.** *Childs Nerv Syst* 2019;35:463–68 [CrossRef Medline](#)
44. Kwan P, Brodie MJ. **Early identification of refractory epilepsy.** *N Engl J Med* 2000;342:314–19 [CrossRef Medline](#)
45. Jeong A, Nakagawa JA, Wong M. **Predictors of drug-resistant epilepsy in tuberous sclerosis complex.** *J Child Neurol* 2017;32:1092–98 [CrossRef Medline](#)
46. Simonyan K, Zisserman A. **Very deep convolutional networks for large-scale image recognition.** *arXiv* 2014;1409:1556 [CrossRef](#)
47. Szegedy C, Liu W, Jia Y, et al. **Going deeper with convolutions.** *arXiv* 2014;1409:4802–98 [CrossRef](#)